Dating Archaeological Strata in the *Magna Mater* Temple Using Solid-state Voltammetric Analysis of Leaded Bronze Coins

Francesca Di Turo[a], Noemí Montoya[b], Joan Piquero-Cilla[b], Caterina De Vito[a], Fulvio Coletti[c], Gabriele Favero[d], María Teresa Doménech-Carbó[e], Antonio Doménech-Carbó*[b]

[a] Department of Earth Sciences, Sapienza University of Rome, P.le Aldo Moro 5, Rome, Italy.
[b] Departament de Química Analítica. Universitat de València. Dr. Moliner, 50, 46100 Burjassot (València) Spain.
[c] Soprintendenza Speciale per il Colosseo, il Museo Nazionale Romano e l'Area Archeologica di Roma, P.zza dei Cinquecento 67, Rome, Italy.
[d] Department of Chemistry and Drug Technologies, Sapienza University of Rome, P.le Aldo Moro 5, Rome, Italy.
[e] Institut de Restauració del Patrimoni, Universitat Politècnica de València, Camí de Vera 14, 46022, València, Spain.

* Corresponding author: e-mail: antonio.domenech@uv.es.

Abstract

The application of solid state electrochemistry techniques for dating archaeological strata using Pb-bearing bronze coins is described. The proposed methodology was applied to samples coming from the Roman archaeological site of *Magna Mater* Temple (Rome, Italy) occurred in different strata dated back between the second half and the end of the 4th century A.D. and the 20th century. The voltammetric signatures of copper and lead corrosion products in contact with aqueous acetate buffer, as well as the catalytic effects produced on the hydrogen evolution reaction, were used for establishing the age of different strata and dating coins belonging to unknown age. Voltammetric data were consistent with a theoretical approximation based on a potential rate law for the corrosion process.

Keywords: Archaeology; Dating; Roman coins; Voltammetry of microparticles; Bronze; Lead.

1 Introduction

In the archaeological frame, determining the provenance of materials and dating artifacts, buildings, etc. are essential analytical objectives for which a variety of physic-chemical methods, including radioactive series, luminescence techniques, among others, are available [1,2]. In many cases, the target is to date the different strata which can be distinguished in a given archaeological site. This is frequently made difficult by the limited number and/or characteristics of the objects accessible in each stratus and/or the complexity of the stratigraphic distribution and/or the appearance of inclusions, and reused materials.

By the first token, dating metals is particularly difficult and typically can only be performed by means of the ^{14}C radiocarbon method in cases where the metal sample was accompanied by organic matter [1,2]. Although relevant data for determining metal provenance can be derived from the chemical composition of the alloy, isotope ratios, and the microstructure of the alloy and patina from metallographic cross sections [3,4], sampling the metal core of the archaeological objects is in general not allowed so that analytical data have to be extracted from metal corrosion patina [5-8].

In this context, Robbiola and Hurtel [9] and Welter [10] proposed that the relation between the Zn/Cu and Sn/Cu concentrations in the patina and the base alloy may act as chronological indicators for brass and bronze artifacts, whereas Reich et al. [11] described a method for dating lead using measurements of the Meissner effect. Such methods, generically, are based on monitoring the corrosion processes involving by the one hand decuprification, destannification and dezincification of bronze/orichalcum in bronze corrosion [12,13] and the growth of metal corrosion products.

Electrochemical techniques are widely used in corrosion studies and have been applied to identify metal alloys and corrosion products [14,15], quantization [16], characterizing metal patinas [17,18], and monitor stabilization processes of archaeological metal [19]. In previous works, we described electrochemical methods for dating lead [20] and copper/bronze [21] archaeological artifacts based on the voltammetry of immobilized microparticles (VIMP), a solid-state technique based on the record of voltammetric response of a solid micro- or nanosample mechanically transferred to the surface of an inert electrode immersed into a suitable electrolyte [22-24]. As a direct antecedent, the proposal by Scholz, Brainina et al. [25] of an electrochemical method for dating ceramics based on electrocatalytic effects of such materials on selected redox probes, as recently reviewed [26]. The

use of VIMP is of particular interest in the field of metal archaeology by its inherent possibility of using sampling at the nanogram level using minimally invasive one-touch sampling protocols [14,27-29].

In a previous work, we have reported a VIMP-based method for dating leaded bronze archaeological artifacts which was applied to statuary and other objects based on the relative intensity of the voltammetric signals of copper and lead corrosion products [30]. Here, we extend the above approach i) providing a detailed analysis of in-depth distribution of Cu and Pb corrosion products, and ii) combining the above signals with those associated to catalytic effects on the hydrogen evolution reaction (HER) for dating purposes.

Here the proposed methodology is applied for dating different archaeological strata in the old rooms of the temple of *Magna Mater* in Rome. This temple, located in the south-west of Palatine, was constructed in 191 B.C and dedicated to the Phrygian divinity Cybele. Lately, the temple was destroyed by fire twice and then, rebuilt by Augustus in 3 A.D. The site, after the temporary abandonment in 410 A.D., was reused until the 17^{th} century A.D. As a result, the site presents a complicated structure constituted by five strata whose ages have been roughly estimated on the basis of archaeological data, namely: A: end of 4^{th} century A.D.; B: end of 5^{th} century A.D.; C: 15^{th} – 17^{th} century A.D.; D: 18th – 20^{th} century A.D. and E: uncertain dating [31]. It is pertinent to note that the crisis and the fall of some regions of the Empire between the 5^{th} and 7^{th} centuries resulted in the loss of access to sources of raw materials such as Sn deposits of Britain, required for the coinage of bronze currency, thus favoring the recast and reuse of Pb during the Late Empire [31].

For establishing a refined dating, a model of moderate corrosion of leaded bronze is presented, extending previous formulations developed for characterizing corrosion products [32,33] and screening copper/bronze monetary emissions [34-37]. The model has been applied to a series of 38 coins which where unearthed in a *latrina*, located on the south side of the *domus Tiberiana*, providing from the different strata previously indicated. In a precedent VIMP plus EIS study on a sub-set of 15 coins from this site [35], we described the possibility of using this methodology for grouping coins from different archaeological strata, thus correlating the voltammetric features associated to cuprite and tenorite corrosion products. VIMP data have been complemented with Raman spectroscopy and focusing ion beam-field emission scanning electron microscopy with energy dispersive x-ray detection (FIB-FESEM-EDX).

The numismatic characteristics of the studied set of coins are summarized in Table 1. The coins, with very few exceptions, were of the types *Aes* 3 and 4 which were common during the 4th century A.D. and still circulating during the last part of the 5th century A.D, under the emperors of *Costantinidi* family Costanzo II (337-361 A.D) and Graziano (colleague in the diarchy with Teodosio I).[35] However, the coins resulted oldest than the deposition's date, gathering around the first half of the 4th century (kingdom of Costanzo II, Valentiniano and Valente), thus denoting a protracted reuse of the currency. This feature, associated to the collapse of the Western Roman Empire, suggests that the Roman coins were the only ones available on monetary circulation in the Middle Age. Accordingly, the disposal of a dating of the different strata in which the coins were unearthed was of significant importance for assessing the hypothesis of the prolonged use of the Roman currency.

2 Experimental

2.1 Instrumentation and methods

Voltammetry of microparticles experiments were performed at sample-modified paraffin-impregnated graphite electrodes using commercial graphite bars (Faber Castell HB, 2.0 mm diameter) using 0.25 M HAc/NaAc buffer at pH 4.75 aqueous solutions as supporting electrolytes. All electrochemical measurements were carried out using a CH I660 potentiostat. A standard three-electrode arrangement was used with a platinum auxiliary electrode and a Ag/AgCl (3M NaCl) reference electrode.

Raman spectra of different coins were obtained by means of a XPlora Horiba MTB model and a 532 nm laser as excitation with maximum power of 90 mW. The samples were measured in backscattering geometry at room temperature. A 100 confocal microscope objective was used to focus the excitation laser on the sample and collect the scattered light to the spectrometer. More than 3 different areas were analyzed per sample, to obtain representative results. Exposure time, number of acquisitions and laser power varied among 5 – 20 s, 10 – 50 and 30 – 80 mW, respectively. Data acquisition was carried out with the LabSpec 6 Spectroscopy Suite from Horiba MTB.

Sectioning of trenches and imaging of four coins belonging to different strata (550602, RZ5814, 550588 and 550612) were performed with a FIB-FESEM Zeiss (Orsay Physics Kleindiek Oxford Instruments) model Auriga compact equipment. FIB-FESEM enabled the semi-quantitative characterization of the microtexture and mineral phases in the superficial corrosion layer and in the inner metal of the bronze coins. The operating conditions were: voltage, 30 kV and current intensity, 500 µA and 20 nA in the FIB for generating the focused beam of Ga ions and a voltage of 3 kV in the FESEM for photographs. X-ray linescans were performed in the trench operating with an Oxford-X Max X-ray microanalysis system coupled to the FESEM controlled by Aztec software. A voltage of 20 kV and a working distance of 6–7 mm were used.

2.2 Samples

A series of 37 Roman coins (catalogue numbers and numismatic description are summarized in Table 1) and a *Tessera* (catalogue number 550581) found in the old rooms of the temple of *Magna Mater*, were studied here. The coins where unearthed by the *Soprintendenza Speciale per il Colosseo, il Museo nazionale Romano e l'Area Archeologica di Roma* during regular archaeological studies in a *latrina*, located on the south side of the *domus Tiberiana* distributed into five strata: A: end of 4^{th} century A.D.; B: end of 5^{th} century A.D.; C: 15^{th} – 17^{th} century A.D.; D: 18th – 20^{th} century A.D. and E: uncertain dating. The characteristics of the coins are presented as a Supplementary information in Table S.1.

3 Results and discussion

3.1 Organoleptic properties and corrosion products

All studied bronze coins showed a relatively advanced state of corrosion, with a brownish surface extensively covered, in most cases, by a rough, irregular greenish layer. Figure 1 depicts the Raman spectra in different spots of coins 7593 and 550580 in which one can see, individualized, the bands of different copper corrosion products, namely, cuprite (bands at 103, 151, 218, 420 and 630 cm^{-1}), tenorite (bands at 290, 337 and 620 cm^{-1}), and malachite (bands at 154, 176, 268, 349, 432, 535, 1062 and 1500 cm^{-1}) [38-40]. Similarly, the spectra of individual lead corrosion products, namely, cerussite (57, 73,102 and 1051 cm^{-1}), hydrocerussite (1051 cm^{-1}), litharge (82, 147 and 339 cm^{-1}), and massicot (77, 88, 143 and 289 cm^{-1}) were also recorded in different spots of the studied coins [38-40].

3.2 FIB-FESEM-EDX imaging

Aiming to complete the electrochemical results, microscopic analysis using FIB-FESEM-EDX was performed. As previously reported [36,37], this technique can be considered as micro-invasive; the focused beam of Ga ions generate trenches which size is lower than 10 µm, then not detectable at the macroscopic level. Figure 2 shows the secondary electron images of the trenches ca. 10 µm length and ca. 15 µm depth produced by FIB in the region of interest in the coins 550602, RZ5814, 550588 and 550612, respectively belonging to the archaeological strata A, B, C and D. Thanks to this technique, it is possible to study the microstructure of the *patina* and the inner alloy of the samples.

The inner metal seems to be quite homogenous due to a core mainly characterized by Cu (averaged to 90±5 % wt) with a lower % wt of Pb (averaged to 5±2 % wt in the core) and Sn as it possible to verify in Table S.2 and in Figure S.1 of Supplementary materials. The oldest coin (550602, Fig. 2a) shows a more complicated microstructure with a high % wt in Pb that can cause characteristic partings of Cu and Pb.

In the case of coin 550612 (Fig.2d), the fracture can be the responsible of the introduction of some typical elements of soil (Si, P, Cl, Ca, As) since the prolonged burial period of the samples. In the considered coin, Sn is not detected while the % wt of Pb is relatively high in comparison with the other three coins, reaching until 24 % wt in the surface. This can support the idea of the large use of Pb in the Roman bronze alloy. The use of Pb is strictly related to the history, the political and the economic issues of the Roman Empire: lead minerals were largely available in the territory under strict Roman control. On the other hand, Romans lost tine mines located in London or in Salamanca during the German invasion in the fifth century [41]. However, the Romans knew that the variations of elemental composition in bronze could affect its inherent characteristics. In particular, adding lead in the bronze improve machinability by making the production easier.

Regarding the availability of metals deposits in the Roman period, it is possible to note the detection of Ag in coin 550602 (Fig. 2a) in the inner part of the alloy. The mineral Galena (PbS) was largely used for the extraction of Pb and during the Roman empire and the richest region of Galena deposits was Sardinia [42,43]. It is well-known that galena can be a primary source of Ag (argentiferous galena) and it is possible to suppose that the Pb used in this coin was extracted from an argentiferous galena *via* cupellation process did not eliminate completely the Ag from the melted

ore mineral. Moreover, Ag is detected into the deeper part of the microstructure, ruling out the hypothesis that it can be an external element due to the burial environment.

As written above, all the coins shows an inner alloy composition made essentially by Cu that gives back a homogeneous microtexture. Coming closer to the surface, the % wt of Cu is reducing while the % wt became higher. This is confirmed in Figure S.2, where it is shown the variation of Cu and Pb (% wt) vs. the depth. Here, the enrichment of Cu in the inner part of the alloy while Pb increase coming closer the surface *patina* is clearly displayed and it due to a several reasons. This variation is possible because of surface depletion of Pb but also to the obvious insolubility of Pb and Cu at the environmental temperature.

3.3 Voltammetric pattern

Figure 3 depicts the SWVs of samples from the brownish region of coins a,b) 550604, and c,d) 550606 attached to graphite electrodes immersed into 0.25 M HAc/NaAc aqueous solution at pH 4.75. Upon scanning the potential in the negative direction, cathodic signals appear at –0.10 V (C_1) and –0.45 (C_2) and –0.60 V (C_3) vs. Ag/AgCl, preceding the rising current at ca. –0.70 V associated to the hydrogen evolution reaction (HER). In positive-going voltammograms, anodic signals at –0.55 V (A_{Pb}) and ca. 0.0 V, usually consisting of two superimposed signals (A_{Cu}) appear. In agreement with literature [14-19] and previous data [29,30], the peak C_1 corresponds to the proton-assisted reduction of cuprite to copper metal, while the signals C_2 and C_3 can be attributed to the reduction of lead corrosion products. These last signals obscure that for the reduction of tenorite, appearing at ca. –0.40 V [21] and can reflect the presence of more or less compact layers of litharge [20,44-46]. The anodic signals can unambiguously be attributed to the oxidative dissolution of the deposits of lead (A_{Pb}) and copper (A_{Cu}) electrochemically generated at negative potentials as a result of the reduction of the respective corrosion products. Both signals display peak splitting, a feature which can be attributed to the formation of different metallic deposits during the reductive step, as described in literature [47,48]. The voltammograms recorded from spots on the greenish regions of the coins were similar although in general the peak C_1 was enhanced, a feature attributable to the presence of other copper corrosion products (mainly malachite, as denoted by Raman spectra) whose reduction in acetate buffer overlays with that of cuprite.

The presence of lead corresponds to a frequent practice in the antiquity because the addition of lead to bronze lowers the alloy cost and results in an improved fluidity and mould-filling capability [49].

The relatively low solubility of lead into copper results, however, in the appearance of peculiar corrosion patterns consisting of globular lead segregates and unalloyed copper inclusions [50,51]. As a result, the composition of the corrosion patina of leaded bronze is particularly sensitive to changes in the composition and metallographic structure of the base alloy. Then, as previously described [30], under long-term metal corrosion, quasi-equilibrium conditions would be attained without extensive corrosion in the metallic phase(s), the ratio between the thermochemical activities of the corrosion products, assumed to be cuprite (Cu_2O) and litharge (PbO), a_{Cu2O}/a_{PbO}, can be related to the initial composition of the leaded bronze, given by the respective molar fractions of copper and lead, x_{Cu}/x_{Pb}, by means of the relationship:

$$\ln\left(\frac{a_{PbO}}{a_{Cu\,2O}}\right)=\frac{2F}{RT}\left[E^{o}(Cu^{+}/Cu)-E^{o}(\mathrm{Pb}^{2+}/\mathrm{Pb})\right]+\ln\left(\frac{\sqrt{K_s(\mathrm{Cu_2O})}}{K_s(PbO)}\right)+\ln\left(\frac{x_{Pb}}{x_{Cu}}\right) \quad (1)$$

$K_s(Cu_2O)$ and $K_s(PbO)$ being the respective solubility products of the corrosion products. Available thermochemical parameters denote that, even for bronzes containing lead yields below 5% wt, the net amount of lead corrosion products should be clearly larger than those of copper corrosion products. This prediction is consistent with voltammetric data where the $i_p(C_1)/i_p(C_2)$ and $i_p(C_1)/i_p(C_2)$ ratios will be representative of the (copper corrosion products)/(lead corrosion products) ratio. Available data for statuary denoted that the $i_p(C_1)/i_p(C_2)$ ratio increased with the age of the objects [30].

3.4 Modeling in depth distribution of corrosion products

Let us assume that corrosion proceeds via formation of local cells yielding a primary patina of cuprite and litharge subsequently growing and forming a more permeable secondary patina, as described by Robbiola et al. [6] for copper/bronze objects. It will be assumed that in the primary patina/base metal interface it is established the equilibrium $Cu_2O + Pb \leftrightarrows Cu + PbO$ while the secondary patina is progressively enriched in tenorite, whose formation through the aerobic oxidation of cuprite is thermodynamically spontaneous [52,53], and 'porous' lead oxide [20,44,45] (see scheme presented as a Supplementary material, Figure S.2). Assuming that these processes ($Cu_2O + (1/2)O_2 \rightarrow CuO$ and $PbO (+ H_2O) \rightarrow$ 'porous' PbO) proceeds independently, there will be a gradient of concentrations of the different products in the secondary patina. It will be assumed that the number of tenorite grains per volume unit, n_{ten}, will increase from zero in the primary/secondary

patina boundary ($x = \delta$) to a value n_{ten}^{sup} at the external surface of the secondary patina ($x = 0$) whereas the number of cuprite grains per volume unit, n_{cup}, will decrease from its value in the primary patina, n_{cup}^{o}, to a surface value of n_{cup}^{sup}. Now, let us define a non-dimensional depth, z, as $z = 1 - x/\delta$ and assume that there is a potential variation of tenorite (and cuprite) concentration with depth given by $n_{ten} = n_{ten}^{sup} z^{\alpha}$ and $n_{cup} = n_{cup}^{o} - n_{ten}^{sup} z^{\alpha}$. For the previously studied binary cuprite plus tenorite system, the peak current (or peak area) for the signal due to cuprite reduction (C_1) will be [36,37]:

$$i(C_1) = \int_0^z \varepsilon_{cup} S[n_{cup}^{o} - n_{ten}^{sup} z^{\alpha}]dz = \varepsilon_{cup} S\left[n_{cup}^{o} z - \frac{n_{ten}^{sup} z^{1+\alpha}}{1+\alpha} \right] \qquad (2)$$

In this equation, ε_{cup} represents an electrochemical constant depending on the electrolyte, potential scan rate, etc. In turn, it will be assumed that the number of 'impermeable' litharge grains per volume unit, n_{lit}, vary with depth following a potential law.

Now, we consider the signals for litharge (assumed to be the main corrosion product of lead). Then, the peak current (or peak area) for the signal due to primary litharge reduction (C_2) can be approximated by the expression:

$$i(C_2) = \int_0^z \varepsilon_{lit} S[n_{lit}^{o} - n_{por}^{sup} z^{\beta}]dz = \varepsilon_{lit} S\left[n_{lit}^{o} z - \frac{n_{por}^{sup} z^{1+\beta}}{1+\beta} \right] \qquad (3)$$

where ε_{lit} represents the corresponding electrochemical coefficient of response, n_{lit}^{o} the number of litharge grains per volume unit at the secondary patina/primary patina interface and n_{por}^{sup} the corresponding quantity for 'porous' litharge in the external surface of the secondary patina. Assuming that the formation of 'porous' litharge is not extensive and that the formation of tenorite is much less extensive, one can approximate:

$$\frac{i(C_1)}{i(C_2)} \approx \frac{\varepsilon_{cup}}{\varepsilon_{lit}} \left[\frac{n^o_{cup}/n^o_{lit}}{1 - \frac{n^{\sup}_{por}}{(1+\beta)\varepsilon_{lit} S n^o_{lit}} (i(C_2))^{\beta}} \right] \qquad (4)$$

This equation (4) predicts a relationship between the $i(C_2)/i(C_1)$ ratio and $i(C_2)$ which can be tested.

Notice that the parameters $n^{\sup}_{ten}$, n^{o}_{cup}, $n^{\sup}_{por}$, n^{o}_{lit}, α, β, should be dependent on the composition and metallographic structure of the base metal and the corrosion history of the object under study while, under fixed experimental conditions (graphite electrode, potential scan rate, etc.) ε_{cup}, ε_{lit} and S will be the same for each series of coins. As a result, assuming aging under uniform conditions, one can predict that, i) for a series of coins of identical age but different composition and metallography, different $i(C_2)/i(C_1)$ vs. $i(C_2)$ curved paths should be obtained, and, ii) for a series of coins of identical composition and metallography but different age, different $i(C_2)/i(C_1)$ vs. $i(C_2)$ plots should be obtained. These predictions were consistent with electrochemical data for coin samples from *Magna Mater* temple (*vide infra*).

Additional modeling can be obtained using the stripping peaks corresponding to the oxidative dissolution of the deposits of Cu and Pb formed in electrochemical runs. It has to be accounted, however, that Pb is electrochemically deposited at potentials more negative (see Figure 3) than Cu, so that, under our experimental conditions, Pb is deposited on a Cu-plated graphite electrode. Denoting by N_{Cu}, N_{Ag} the absolute number of Cu and Pb grains electrochemically generated in the microparticulate deposit after sampling at a depth z, one can write: $i(A_{Cu}) = \varepsilon_{Cu} N_{Cu} \approx \varepsilon_{Cu} S[2n^o_{cup} z - n^{\sup}_{ten} z^{1+\alpha}/(1+\alpha)$ and $i(A_{Pb}) = \varepsilon_{Pb} N_{Pb} = \varepsilon_{Pb} S n^o_{lit} z$. Using the above assumptions, one can arrive at the equation:

$$i(A_{Cu}) = \frac{\varepsilon_{Pb}}{\varepsilon_{Cu}} \left[\frac{2n^o_{cup}}{\varepsilon_{Pb} n^o_{lit}} i(A_{Pb}) - \frac{n^{\sup}_{ten}}{(1+\alpha)\varepsilon^{\alpha}_{Pb} n^o_{lit}} (i(A_{Pb}))^{\alpha} \right] \qquad (5)$$

which relates the peak current / peak area of signals A_{Cu} and A_{Pb}.

A third experimental test can be obtained using the current measured for the HER process at a given potential, i(HER). Since this process occurs more easily at Cu- and Pb-plated graphite than at the bare graphite surface, one can assume that the current for this process will result from the sum of two contributions: the H^+ (aq) reduction occurring at the 'free', uncovered graphite surface, and that due to the catalytic effect of the metals deposited in the previous cathodic processes for the reduction of copper and lead corrosion products; i.e.: $i(\mathrm{HER}) = h_{\mathrm{HER}}(S_{\mathrm{o}} - S) + h_{\mathrm{Cu}} n_{\mathrm{Cu}} + h_{\mathrm{Pb}} n_{\mathrm{Pb}}$, where S_{o} denotes the total electrode area and the h-coefficients are characteristic of each process and depend on the electrochemical conditions of operation (pH, scan rate, etc.). Taking into account the previous considerations, one can write:

$$i(\mathrm{HER}) = h_{\mathrm{HER}}(S_{\mathrm{o}} - S) + \frac{(2h_{Cu} n^{o}_{cup} + h_{Pb} n^{o}_{lit})}{\varepsilon_{lit} n^{o}_{lit}} i(C_2) - S^{\alpha} h_{Cu} \frac{n^{\mathrm{sup}}_{ten} (i(C_1))^{1+\alpha}}{(1+\alpha)\varepsilon^{1+\alpha}_{lit}} \qquad (6)$$

which relates i(HER) with $i(C_2)$ and can also be experimentally tested. See Supplementary information (Annex A.1) for detailed derivation of Eqs. (5) and (6).

3.5 Dating

Figure 4a depicts the $i(C_2)/i(C_1)$ vs. $i(C_2)$ plots for coins recovered in the stratus A of *Magna Mater* temple. In agreement with previous results on different 19th century Chinese [36] and 17th century Spanish [37] series of coins, there is possibility of discriminating between different sets of samples. The representation of the entire set of data (Supplementary information, Figure S.3) permits to divide the studied coins in three groups so that the distribution of data points clearly differ from the oldest strata, dated back to 4th A.D. (a) and 5th A.D. (B) to the strata attributed to the 15th-17th (C) and 18th-20th (D) A.D. centuries whereas data points for coins from the level E, of uncertain chronology, fall in a narrow region close to that occupied by data points of coins in A and B levels. Discrimination between different sub-sets of coins can also be obtained from stripping peaks, as can be seen in Figure 5b in which the variation of $i(A_{Pb})$ vs. $i(A_{Cu})$ for coins recovered in the stratus A of *Magna Mater* temple is shown (data from 2-4 spots in each coin are represented). In both representations, coins of Constanzo (550580 and 550602) and Constantino and Valente (550584, 550585 and 550601) defined two clearly separated tendency lines consistent with Eqs. (4) and (5) in turn separated from a third tendency line where data points for coins 550583 and 550604 were grouped. Only the first was identified as coined by Graziano, thus suggesting that the second can be ascribed to the same production.

Similar sample screening was obtained in the other strata (Figure 5), corresponding to the variation of a) $i(C_2)/i(C_1)$ on $i(C_2)$ and b) i(HER) vs. $i(C_2)$ for coins recovered in the stratus D. Here, the coins of Domiziano (550615) and Valentiniano (D7594) defined a common tendency line, whereas the coins from Valente (550614) and Valentiniano (550612 and 7593) defined another tendency line clearly separated from the above. Unassigned coins 550590, RZO, 550616 and 550617 showed an electrochemical behavior entirely consistent with that of the coins of this second group.

Comparing the voltammograms of coins of the same numismatic series, there is a clear distinction between those recovered in the different archaeological strata. This can be seen in Figure 6 where a double logarithmic representation of $i(C_2)/i(C_1)$ vs. $i(C_2)$ for coins of the emperors Constanzo and Constante from strata A, B, C and D is plotted. Clearly, the coins from the different levels fall in different tendency lines ordered according to a crescent age of the strata.

Assuming that a potential rate law applies for the evolution of the corrosion products of copper and lead under uniform conditions of aging [11,20,21], consistent with long-term metal corrosion studies [54], we already proposed a simple equation to describe the ratio between the amounts of secondary corrosion products of copper and lead, derived from voltammetric measurements, can be expressed as [30]:

$$\frac{i_{\mathrm{p}}(\mathrm{C}_1)}{i_{\mathrm{p}}(\mathrm{C}_2)} \approx \frac{x_{\mathrm{Cu}}}{x_{\mathrm{Pb}}} = \frac{[X_{\mathrm{Cu}} / X_{\mathrm{Pb}} + k^*_{\mathrm{Cu}} t]^{\alpha}}{[1 + k^*_{\mathrm{Pb}} t]^{\alpha}} \qquad (7)$$

so that a calibration graph can be constructed from voltammetric data using a set of samples of known age. In the above equation, k^*_{Cu}, k^*_{Pb}, represent the rate constants for the formation copper and lead corrosion products in the secondary patina and X_{Cu}, X_{Pb}, the initial concentration of such products at the beginning of the corrosion process, in principle equivalent to the composition of the base metal alloy.

The above equation has the drawback of the low values of $i_{\mathrm{p}}(C_1)$ current. A plausible alternative is the use of the current recorded at a given potential for the HER process. Assuming that $n^o_{cup} \approx i(C_1)/\varepsilon_{cup} Sz$ and $n^o_{lit} \approx i(C_2)/\varepsilon_{lit} Sz$, and neglecting tenorite formation, Eq. (6) becomes:

$$i(\mathrm{HER}) \approx h_{\mathrm{HER}}(S_o - S) + Sz(2h_{Cu}n^o_{cup} + h_{Pb}n^o_{lit}) \qquad (8)$$

Since, under our experimental conditions, the coverage of the graphite electrode is low, one can assume that $S << S_o$. Introducing the HER current measured at the bare graphite electrode, i^o(HER), the increment of HER current will be:

$$\Delta i(\mathrm{HER}) = i(HER) - i^o(HER) \approx i(HER) - h_{\mathrm{HER}}S_o \qquad (9)$$

Then, the ratio between the surface concentrations of cuprite and tenorite can be expressed as (for details, see Supplementary information, Annex A.1):

$$\frac{n^o_{cup}}{n^o_{lit}} = \frac{\Delta i(HER)}{i(C_2)}\frac{\varepsilon_{lit}}{2h_{Cu}} - h_{Pb} \qquad (10)$$

Assuming, as before, that cuprite and litharge evolve independently with time, one can obtain the dating equation:

$$\frac{\Delta i(HER)}{i(C_2)} = h_{Pb} + \frac{2h_{Cu}}{\varepsilon_{lit}}\frac{[X_{\mathrm{Cu}}/X_{\mathrm{Pb}} + k^*_{\mathrm{Cu}}t]^{\alpha}}{[1 + k^*_{\mathrm{Pb}}t]^{\alpha}} \qquad (11)$$

For constructing calibration graphs, average values of the peak currents $i(C_1)$ and $i(C_2)$ and the HER current at –0.85 V from 3-5 spots on each sample were taken. Given the relatively smooth variation of these values on the amount of sample and taking into account the relatively high uncertainty in such quantities (see Figures 4-6), this procedure yields a reasonable estimate of the correlation between the $i(C_1)/i(C_2)$ and $\Delta i(\mathrm{HER})/i(C_2)$ ratios and the corrosion time t. Figure 7 depicts the representation of $i(C_1)/i(C_2)$ vs. time using data from leaded bronze statuary (grey rectangles) which can be fitted to theoretical curves for lead contents between 5 and 15 % wt inserting $\alpha = 0.93$, $k^*_{Cu} = 1.0 \times 10^{-3}$ years^{-1} and $k^*_{Pb} = 1.0 \times 10^{-1}$ years^{-1} into Eq. (7). Satisfactory calibration was also obtained using the representation of $\Delta i(\mathrm{HER})/i(C_2)$ vs. t, depicted in Figure 8, taking the above parameters and adding before, $h_{\mathrm{Pb}} = 0.080$ and $2h_{\mathrm{Cu}}/\varepsilon_{\mathrm{lit}} = 0.57$ into Eq. (11). Comparison of

experimental data for the $i(C_1)/i(C_2)$ and $\Delta i(HER)/i(C_2)$ ratios determined for *Magna Mater* coins with calibration graphs indicates:

a) Coins of level A of Graziano (367-383), Constantino II (347-348), Constanzo and Constante (337-341) and Valente (375-378) were inserted in the diagram just corresponding to their age, thus acting in confirmation of archaeological data attributing this stratus to the 2nd half of the 4th century A.D.

b) The apparent age of coin RZ5814, a *Folles* of Constanzo minted in Roma in 335-337 A.D. recovered in the level B, was ca. 100 years younger, thus confirming the attribution of this level to the 5th century A.D. [31].

c) The averaged age of coins from level C can be estimated as 500±100 years, consistent with archaeological dating between the 15th and 17th centuries.

d) Coins from the stratus D corresponded to apparent ages of 350±50 years, in agreement with the attribution of this level to a time interval between the 18th and the 20th centuries.

e) Coins found in the stratigraphic level E (550582, D7564, RZ6708 and RZ6720) were, as deduced from their position in the $i(C_1)/i(C_2)$ vs. $i(C_2)$ diagrams, buried during a period of time equivalent to that of coins of the level A, thus suggesting that, at least in the zone in which such coins were recovered, the age was ca. 4th century A.D.

4 Conclusions

The solid state voltammetric response of leaded bronze nanosamples from a series of 37 Roman coins found in the old rooms of the temple of *Magna Mater* (south-west of Palatine, Rome) attached to graphite electrodes in contact with aqueous acetate buffer at pH 4.75 consisted of well-defined signals denoting the presence of cuprite and litharge as main corrosion products. Electrochemical data, supported by Raman spectroscopy and FIB-FESEM, suggested that the corrosion process involved the growth of a secondary patina of porous litharge and cuprite plus tenorite over the primary patina of cuprite plus impermeable litharge. The relationship between the cathodic signals for the reduction of copper and lead corrosion products, as well as the relationship between the anodic signals for the stripping of copper and lead and the relationship of such signals with the current for the hydrogen evolution reaction were used to discriminate between different archaeological strata.

Voltammetric data were consistent with calibration graphs for dating leaded bronze and permitted a refined dating of the different archaeological strata, thus illustrating the capabilities of solid state voltammetry for yielding archaeometric information.

Ackonwledgements: Financial support from the MINECO Projects CTQ2014-53736-C3-1-P and CTQ2014-53736-C3-2-P which are supported with ERDF funds is gratefully acknowledged. PhD grants of the Department of Earth Sciences, Sapienza University of Rome, are gratefully thanked.

References

[1] M. J. Aitken, *Science-Based Dating in Archaeology*. Longman, New York, chapter 8.

[2] M. A. Geyh, H. Schleicher, *Physical and Chemical Dating Methods and Their Application*. Springer, Berlin-Heidelberg, 1990.

[3] D. Attanasio, G. Bultrini, G. M. Ingo, *Archaeometry* **2001**, *43*, 529.

[4] I. Constantinides, A. Adriaens, F. Adams, *Appl. Surf. Sci.* **2002**, *189*, 90.

[5] D. A. Scott, *J. Am. Ite. Cons.* **1994**, *33*, 1.

[6] L. Robbiola, J. –M. Blengino, C. Fiaud, C. *Corr. Sci.* **1998**, *40*, 2083.

[7] L. Robbiola, R. Portier, *J. Cult. Herit.* **2006**, *7*, 1.

[8] C. Chiavari, K. Rahmouni, H. Takenouti, S. Joiret, P. Vermaut L. Robbiola, *Electrochim. Acta* **2007**, *52*, 7760.

[9] L. Robbiola, L. –P. Hurtel, Standard nature of the passive layers of buried archaeological bronze - The example of two Roman half-length portraits, in *METAL 95*, MacLeod, I.; Pennec, S.; Robbiola, L. Eds., James & James Science Publ., London, pp. 109–17.

[10] J. –M. Welter, *Techné* **2003**, 18, 27–36.

[11] S. Reich, G. Leitus, S. Shalev, *New J. Phys.* **2003**, *5*, 99.1.

[12] I. De Ryck, A. Adriaens, E. Pantos, F. Adams, *Analyst* **2003**, *128*, 1104.

[13] J. Cura D'Ars de Figueiredo Junior, V. de Freitas Cunha Lins, V. M. De Bellis, *Appl. Surf. Sci.* **2007**, *253*, 7104.

[14] V. Costa, K. Leyssens, A. Adriaens, N. Richard, F. Scholz, *J. Solid State Electrochem*. **2010**, *14*, 449.

[15] D. Satovic, S. Martinez, A. Bobrowski, *Talanta* **2010**, *81*, 1760.

[16] F. Arjmand, A. Adriaens, *J. Solid State Electrochem*. **2012**, *16*, 535.

[17] N. Souissi, L. Bousselmi, S. Khosrof, E. Triki, *Mater. Corros*. **2004**, *55*, 284.

[18] M. Serghini-Idrissi, M. C. Bernard, F. Z. Harrif, S. Joiret, K. Rahmouni, A. Srhiri, H. Takenouti, V. Vivier, M. Ziani, *Electrochim. Acta* **2005**, *50*, 4699.

[19] K. Leyssens, A. Adriaens, C. Degrigny, E. Pantos, *Anal. Chem*. **2006**, *78*, 2794.

[20] A. Doménech-Carbó, M. T. Doménech-Carbó, M. A. Peiró-Ronda, *Anal. Chem*. **2011**, *83*, 5639.

[21] A. Doménech-Carbó, M. T. Doménech-Carbó, S. Capelo, T. Pasíes-Oviedo, I. Martínez-Lázaro, *Angew. Chem. Int. Ed*., **2014**, *53*, 9262.

[22] F. Scholz, B. Meyer, Voltammetry of solid microparticles immobilized on electrode surfaces in *Electroanalytical Chemistry, A Series of Advances*, A. J. Bard, I. Rubinstein, Eds, Marcel Dekker, New York, 1998, vol. 20, pp. 1–86.

[23] F. Scholz, U. Schröder, R. Gulaboski, A. Doménech-Carbó, *Electrochemistry of Immobilized Particles and Droplets*, 2nd edit. Springer, Berlin-Heidelberg, 2014.

[24] A. Doménech-Carbó, J. Labuda, F. Scholz, *Pure Appl. Chem*. **2013**, *85*, 609.

[25] F. Scholz, U. Schröder, S. Meyer, Kh. Z. Brainina, N. F. Zakharchuk, N. V. Sobolev, O. A. Kozmenko, *J. Electroanal. Chem*. **1995**, *385*, 139.

[26] A. Doménech-Carbó, A. *J. Solid State Electrochem*. **2017**, *21*, 1987.

[27] D. Blum, W. Leyffer, R. Holze, *Electroanalysis* **1996**, *8*, 296.

[28] A. Doménech-Carbó, M. T. Doménech-Carbó, V. Costa, *Electrochemical methods applied to archaeometry, conservation and restoration*, Monographs in Electrochemistry Series, F. Scholz, Edit, Springer, Berlin-Heidelberg, 2009.

[29] A. Doménech-Carbó, M. T. Doménech-Carbó, M. A. Peiró-Ronda, *Electroanalysis* **2011**, *23*, 1391.

[30] A. Doménech-Carbó, M. T. Doménech-Carbó, J. Redondo-Marugán, L. Osete-Cortina, J. Barrio, A. Fuentes, M. V. Vivancos-Ramón, W. Al-Sekhaneh, B. Martínez, I. Martínez-Lázaro, T. Pasíes-Oviedo, *Archaeometry*, in press, DOI: 10.1111/arcm.12308.

[31] F. Coletti, *L'obolo della dea: monete dai contesti di vita, abbandono e distruzione dell'area sud ovest del Palatino*, Soprintendenza Speciale per il Colosseo, il Museo Nazionale Romano e l'Area Archeologica di Roma, 2015.

[32] A. Doménech-Carbó, M. T. Doménech-Carbó, T. Pasíes-Oviedo, M. C. Bouzas-Bello, *Electroanalysis* **2011**, *23*, 2803.

[33] A. Doménech-Carbó, M. T. Doménech-Carbó, J. Redondo-Marugán, L. Osete-Cortina, M. V. Vivancos-Ramón, *Electroanalysis* **2016**, *28*, 833.

[34] A. Doménech-Carbó, M. T. Doménech-Carbó, T. Pasíes-Oviedo, M. C. Bouzas-Bello, *Electroanalysis* **2012**, *24*, 1945.

[35] F. Di Turo, N. Montoya, J. Piquero-Cilla, C. De Vito, F. Coletti, G. Favero, A. Doménech-Carbó, *Anal. Chim. Acta* **2017**, *955*, 36.

[36] A. Doménech-Carbó, M. T. Doménech-Carbó, E. Montagna, C. Álvarez-Romero, Y. Lee, *Talanta* **2017**, *169*, 50.

[37] A. Doménech-Carbó, M. T. Doménech-Carbó, C. Álvarez-Romero, N. Montoya, T. Pasíes-Oviedo, M. Buendía-Ortuño, *Electroanalysis*, in press. DOI: 10.1002/elan.201700326.

[38] L. Burgio, R. J. H. Clark, *Spectrochim. Acta A* **2001**, *57*, 1491.

[39] E. Basso, C. Invernizzi, M. Malagodi, M. F. La Russa, D. Bersani, P. P. Lottici, *J. Raman Spectrosc*. **2014**, *45*, 238.

[40] M. C. Caggiani, A. Cosentino, A. Mangone, *Microchem. J*. **2016**, *129*, 123.

[41] J. C. Edmonson, *J. Roman Stud*. **1989**, *79*, 84.

[42] R. H. Tykot, Bronze, sea and Sardinia: social and technological evolution in an island society, in *Proc. Int. Conf. Metals in Antiquity*, Harvard University, 10–13 September 1997.

[43] T. De Caro, C. Riccucci, E. I. Parisi, F. Faraldi, D. Caschera, *Appl Phys A* **2013**, *113*, 945.

[44] D. Pavlov, B. Monakhov, K. Salmi, G. Sundholm, *Electrochim. Acta*, **1991**, *36*, 953.

[45] W. –B. Cai, Y. –Q. Wan, H. –T. Liu, W. –F. Zhou, *J. Electroanal. Chem.* **1995**, *387*, 95.

[46] N. Zakharchuk, S. Meyer, B. Lange, F. Scholz, *Croat. Chem. Acta* **2000**, *73*, 667.

[47] S. Komorsky-Lovric, M. Lovric, A. M. Bond, *Anal. Chim. Acta* **1992**, *258*, 299.

[48] M. De Keersmaecker, M. Dowsett, R. Grayburn, D. Banerjee, A. Adriaens, *Talanta* **2015**, *132*, 760.

[49] M. J. Hughes, J. P. Northover, B. E. P. Staniaszek, *Oxford Journal of Archaeology* **1982**, *3*, 359.

[50] G. M. Ingo, P. Plescia, E. Angelini, C. Riccucci, T. De Caro, *Appl. Phys. A* **2006**, *83*, 611.

[51] M. Quaranta, E. Catelli, S. Prati, G. Sciutto, R. Mazzeo, *J. Cult. Herit.* **2014**, *15*, 283.

[52] D. A. Scott, *Stud. Conservat.* **1997**, *42*, 93.

[53] M. T. S. Fair, L. Guerrero, O. L. Arenas, P. K. Fair, *Appl. Surf. Sci*. **1999**, *150*, 143.

[54] G. M. Ingo, E. Angelini, G. Bultrini, I. Calliari, M. Dabala, T. De Caro, *Surf. Interf. Anal*. **2002**; *34*, 337.

FIGURES

Figure 1. Raman spectra of different spots in coins a-d) 7593 and e-g) 550580 characterizing the presence of malachite (a), cuprite (b), cerussite (c), hydrocerussite (d) tenorite (e), litharge (f) and massicot (g). Insets: photographic images of these coins.

Figure 2. Secondary electron images of trench ca. 10 μm length and ca. 15 μm depth generated by FIB on coins: a) 550602 b) RZ5814 c) 550588 d) 550612.

Figure 3. SWVs of samples from the brownish region of coins: a,b) 550604, and c,d) 550606 attached to graphite electrodes immersed into 0.25 M HAc/NaAc aqueous solution at pH 4.75. Potential scan initiated at a,c) +0.75 V in the negative direction and b,d) –0.75 V in the positive direction; potential step increment 4 mV; square wave amplitude 25 mV; frequency 5 Hz. Two or three replicate measurements on different areas of the coin surface are superimposed.

Figure 4. Variation of a) $i(C_2)/i(C_1)$ on $i(C_2)$ and b) $i(A_{Pb})$ vs. $i(A_{Cu})$ for coins recovered in the stratus A of *Magna Mater* temple from SWVs such as in Figures 3. Triangles: Graziano emperor, coin 550583, and coin 550604; solid squares: *aes* of Constantino and Valente emperors (550584, 550585 and 550601 coins); squares: Constanzo emperor (550580 and 550602 coins).

Figure 5. Variation of a) $i(C_2)/i(C_1)$ on $i(C_2)$ and b) i(HER) vs. $i(C_2)$ for coins recovered in the stratus D of *Magna Mater* temple measured in SWVs such as in Figures 3a,c. Squares: coin of Domiziano (550615), Valentiniano (D7594) and unassigned coins 550590, RZO, 550616 and 550617; solid squares: Valente (550614) and Valentiniano (550612 and 7593) coins.

Figure 6. Double logarithmic representation of $i(C_2)/i(C_1)$ vs. $i(C_2)$ for coins of the emperors Constanzo and Constante recovered in the levels A (550580, 550602), B (RZ5814), C (580588, 580597) and D (7593, 550612).

Figure 7. Variation of $\log[i(C_1)/i(C_2)]$ with the corrosion time. Comparison of theoretical lines for different selected compositions of leaded bronze inserting $k^*_{Cu} = 1.0 \times 10^{-3}$ years^{-1} and $k^*_{Pb} = 1.0 \times 10^{-1}$ years^{-1} into Eq. (7) and experimental data from leaded bronze statuary in ref. [30] (grey rectangles) and leaded bronze coins in this study (white rectangles).

Figure 8. Calibration graph of $\Delta i(\mathrm{HER})/i(C_2)$ vs. corrosion time. Comparison of theoretical lines for different selected compositions of leaded bronze inserting $k^*_{Cu} = 1.0 \times 10^{-3}$ years^{-1} and $k^*_{Pb} = 1.0 \times 10^{-1}$ years^{-1} into Eq. (11) and experimental data for leaded bronze coins from the Magna Mater temple.

Figure 1.

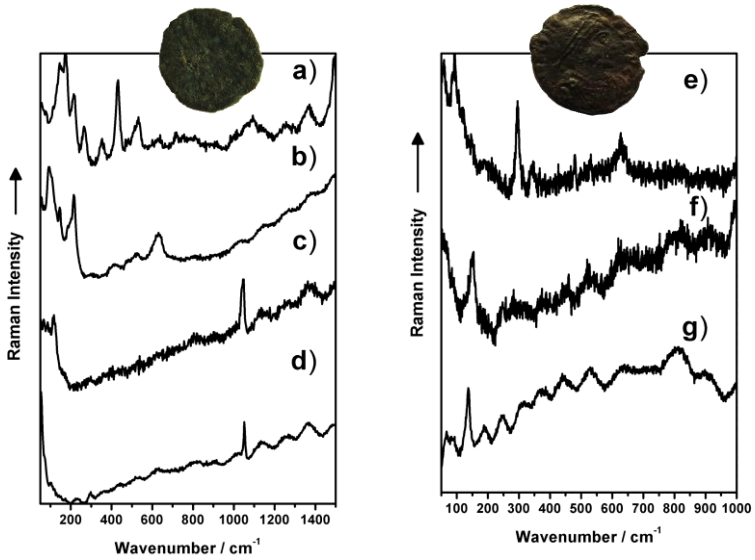
a)
b)
c)
d)
Raman Intensity
200 400 600 800 1000 1200 1400
Wavenumber / cm-1
e)
f)
g)
Raman Intensity
100 200 300 400 500 600 700 800 900 1000
Wavenumber / cm-1

Figure 2.

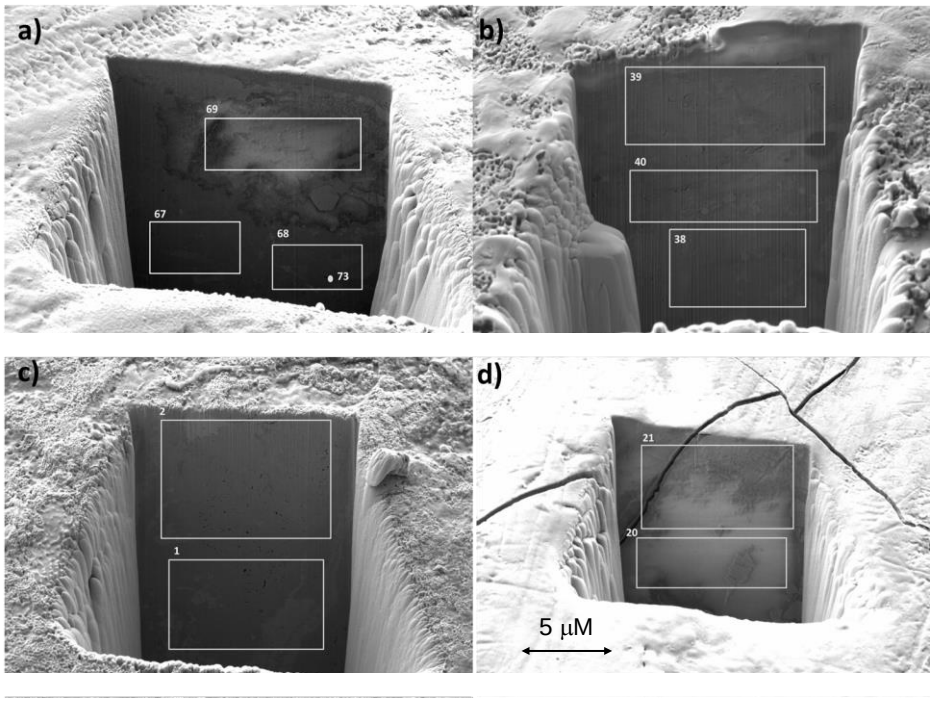

Figure 3.

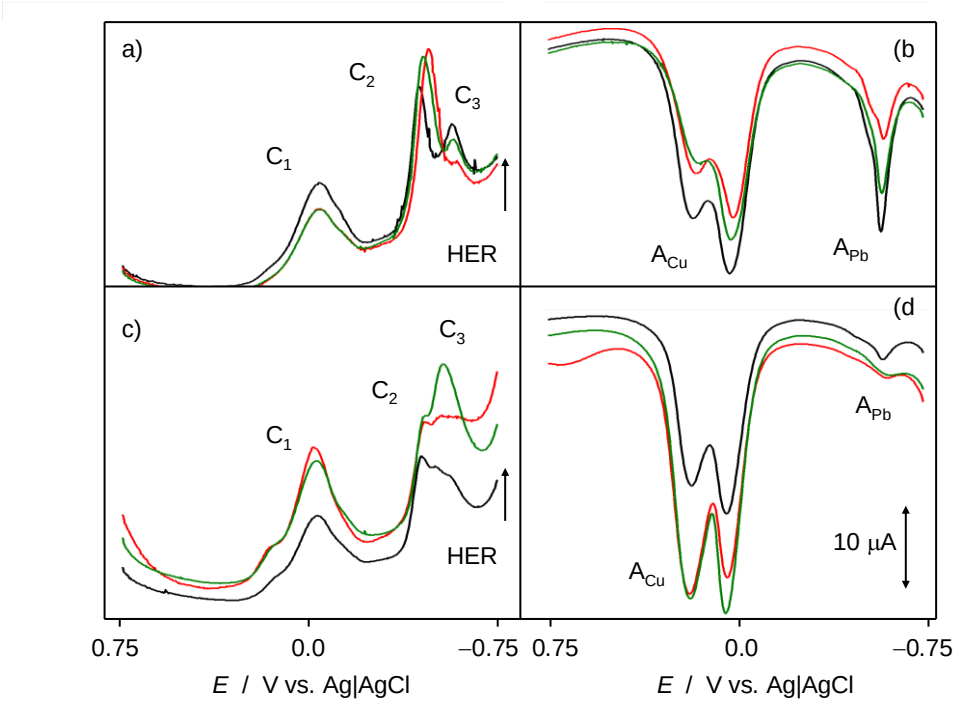
a)
C1
C2
C3
HER
(b
ACu
APb
c)
C3
C2
C1
HER
(d
APb
10 µA
ACu
0.75
0.0
–0.75
E / V vs. Ag|AgCl
0.75
0.0
–0.75
E / V vs. Ag|AgCl

Figure 4.

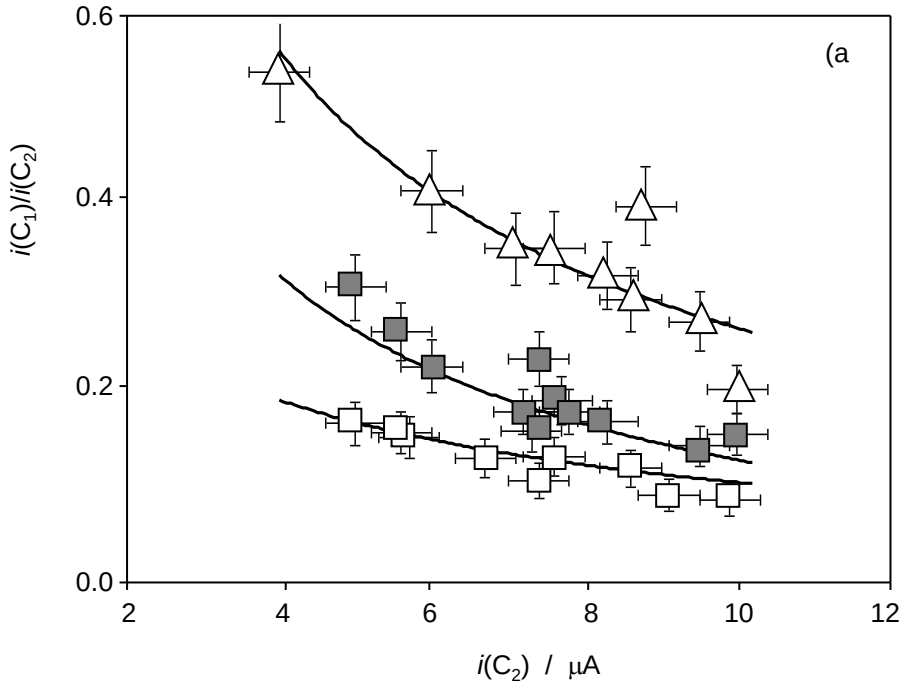
(a
0.6
0.4
0.2
0.0
2
4
6
8
10
12
$i(C_1)/i(C_2)$
$i(C_2)$ / μA

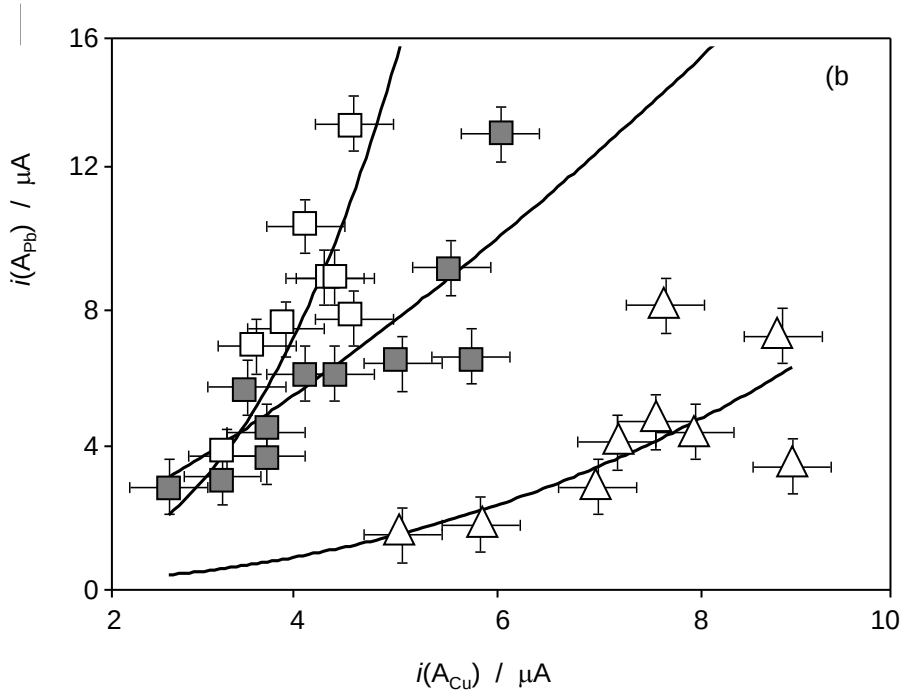
(b
16
12
8
4
0
2
4
6
8
10
$i(A_{Pb})$ / μA
$i(A_{Cu})$ / μA

Figure 5.

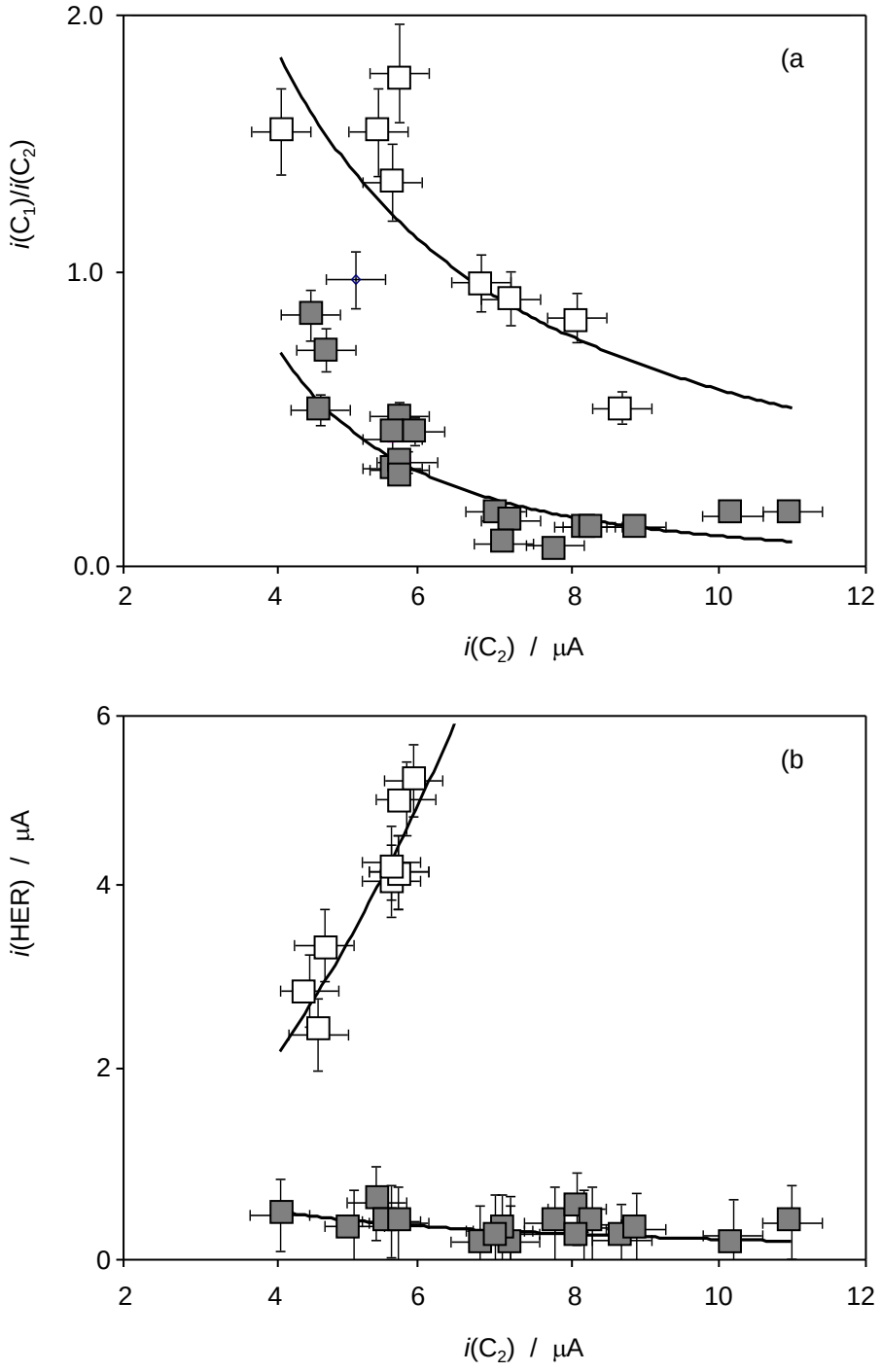
(a
2.0
1.0
0.0
$i(C_1)/i(C_2)$
2
4
6
8
10
12
$i(C_2)$ / μA
(b
6
4
2
0
i(HER) / μA
2
4
6
8
10
12
$i(C_2)$ / μA

Figure 6.

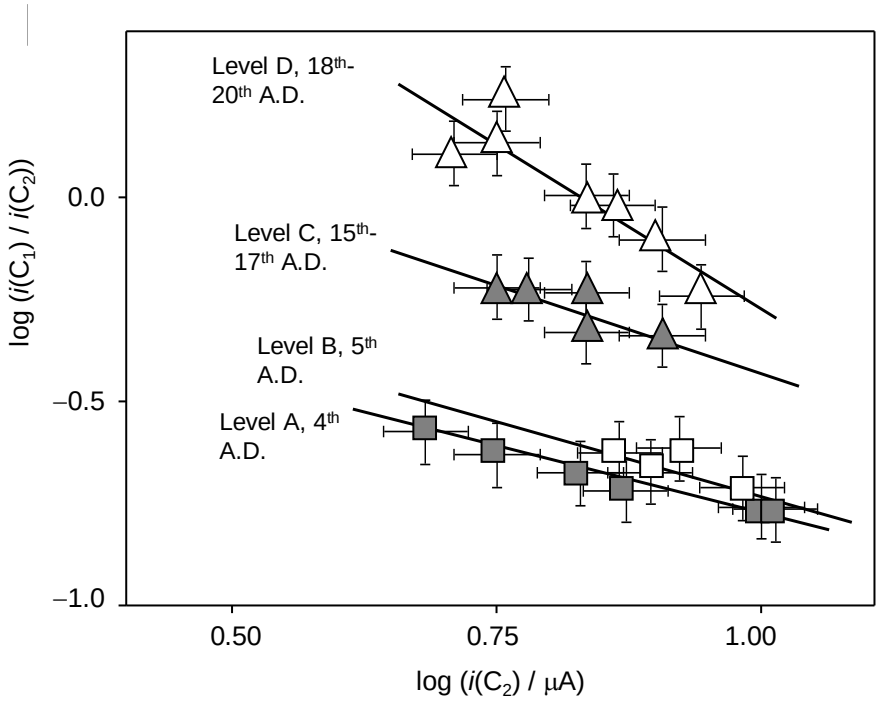
Level D, 18th-20th A.D.
Level C, 15th-17th A.D.
Level B, 5th A.D.
Level A, 4th A.D.
0.0
−0.5
−1.0
0.50
0.75
1.00
log (i(C1) / i(C2))
log (i(C2) / μA)

Figure 7.

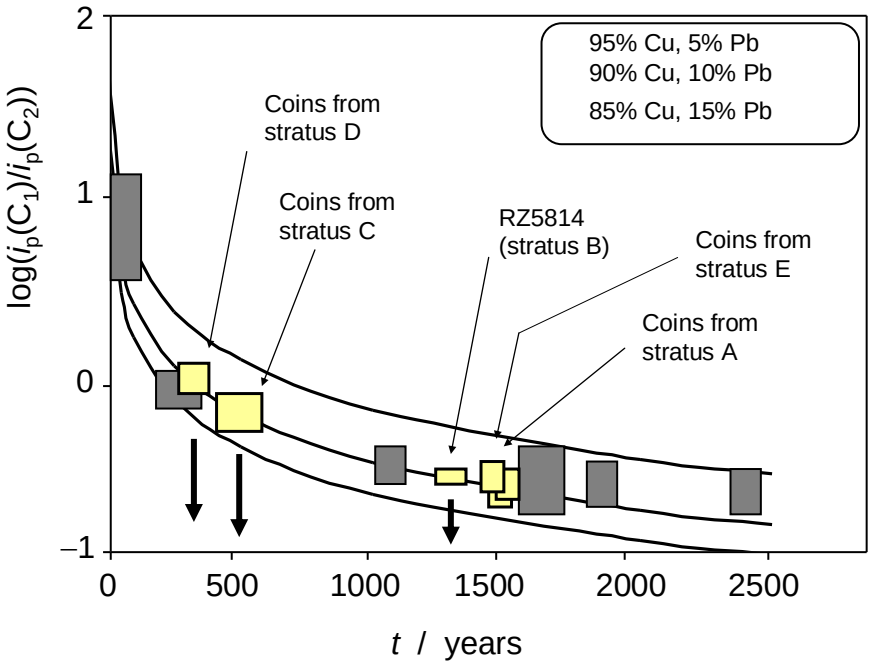
95% Cu, 5% Pb
90% Cu, 10% Pb
85% Cu, 15% Pb
Coins from stratus D
Coins from stratus C
RZ5814 (stratus B)
Coins from stratus E
Coins from stratus A
log(ip(C1)/ip(C2))
t / years
2
1
0
–1
0
500
1000
1500
2000
2500

Figure 8.

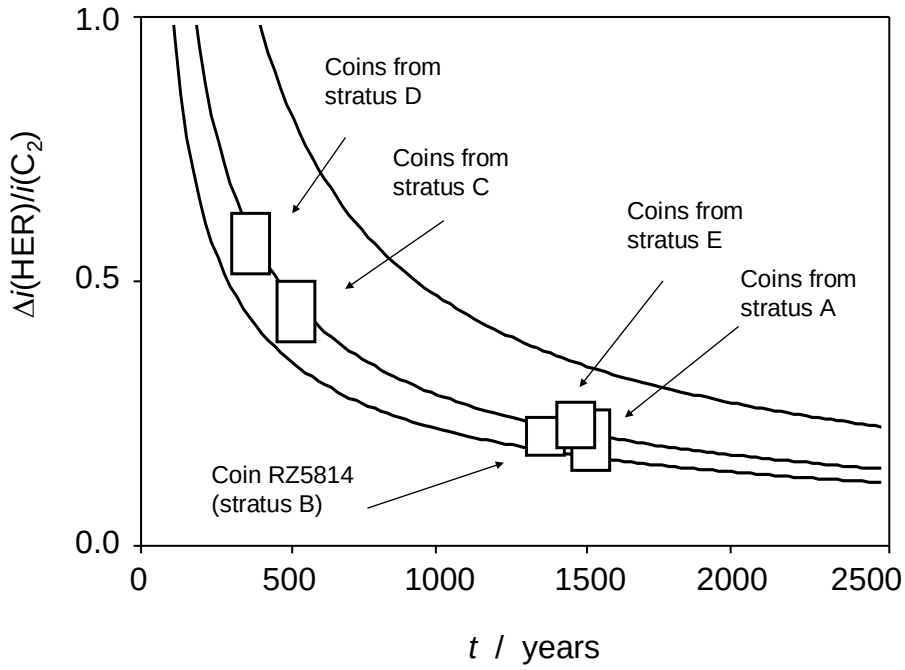
1.0
0.5
0.0
0
500
1000
1500
2000
2500
Δi(HER)/i(C2)
t / years
Coins from stratus D
Coins from stratus C
Coins from stratus E
Coins from stratus A
Coin RZ5814 (stratus B)